

Micro-fabrication of patterned LSCF thin-film cathodes with gold current collectors

N.J. Simrick^{a,*}, J.A. Kilner^a, A. Atkinson^a, J.L.M. Rupp^b, T.M. Ryll^b, A. Bieberle-Hütter^b, H. Galinski^b, L.J. Gauckler^b

^a Department of Materials, Imperial College, London SW7 2BP, UK

^b Nonmetallic Inorganic Materials, ETH Zurich, Switzerland

ARTICLE INFO

Article history:

Received 31 August 2009

Accepted 22 March 2010

Available online 30 April 2010

Keywords:

Micro SOFC

Cathode

LSCF

Polarisation resistance

Fabrication

Patterned

Etching

ABSTRACT

Lanthanum strontium cobalt iron oxide ($\text{La}_{0.6}\text{Sr}_{0.4}\text{Co}_{0.2}\text{Fe}_{0.8}\text{O}_{3-\delta}$) thin films were deposited via pulsed laser deposition on single-crystal yttria-stabilised zirconia (YSZ) substrates and lithographically patterned to produce geometrically well-defined micro-cathodes. The films had low porosity and a mainly columnar microstructure. A minimum LSCF feature size of $20\ \mu\text{m}$ was achieved and a range of designs fabricated for studies of the oxygen reduction reaction. Wet etching in dilute hydrochloric acid and dry etching via Ar^+ sputtering were investigated in order to produce structures with near-vertical side walls and well-defined geometries. Ar^+ sputter-etching yielded structures with side walls inclined at approximately 75° to the substrate and was the preferential choice. Etch rates of $400\ \text{nm}\ \text{min}^{-1}$ and $3.4\ \text{nm}\ \text{min}^{-1}$ were determined for wet and dry etching, respectively. A novel gold current collector geometry was fabricated using photolithography lift-off technique in order to reduce ohmic drops due to the cathode geometry, whilst controlling the LSCF active area and TPB lengths. The deposited LSCF had an electronic conductivity of $5700\ \text{S/m}$ in air and an activation energy, E_A of $0.14\ \text{eV}$. Degradation of LSCF conductivity upon heat cycling was observed for thin films that had been subjected to an etching process, in contrast to shadow mask processed structures.

© 2010 Elsevier B.V. All rights reserved.

1. Introduction

Lanthanum strontium cobalt iron oxide (LSCF) is a state of the art mixed ionic–electronic conducting (MIEC) solid oxide fuel cell (SOFC) cathode material with high ionic and electronic conductivity [1–3]. This has reduced the SOFC operating temperature to below $800\ ^\circ\text{C}$. It is reported in literature that the oxygen reduction reaction at LSCF cathodes occurs via the solid state oxygen diffusion path, but it is the surface reaction which is rate limiting [2,4]. However, it remains to be seen whether or not the surface area of LSCF remains significantly active towards the oxygen reduction at low temperatures to the best of the authors' knowledge. Likewise, one might ask whether or not there is a temperature range over which three-phase boundaries (TPB) become significant in oxygen reduction, if at all. It has also not been shown experimentally whether oxygen reduction via surface oxygen diffusion on thin-film cathode vertical 'side walls' defined by the film thickness can be deemed negligible as suggested by Prestat et al. [4]. The use of geometrically well-defined (gwd) electrodes as in this study for the investigation of fundamental reaction mechanisms is well documented [5,6]. The gwd concept involves the production of a matrix of gwd electrodes of known TPB length, bulk

diffusion length (i.e. film thickness) and active areas that are tested systematically with the aim of correlating such parameters with the performance i.e. polarisation resistance. In such model electrode studies one usually assumes the electrode is dense in order to investigate the material in question without the added complexity of gas-phase diffusion that exists in porous structures [5]. Physical vapour deposition techniques such as sputtering and pulsed laser deposition are generally assumed to provide this but close microstructural examination of deposited films is required to determine the actual density. The production of patterned electrodes is also significant in micro-SOFC development, where the reproducibility of structured thin films is of importance.

The demonstration of patterned LSCF thin film cathodes is evident in the literature for structures consisting of simple square or circular geometries approximately $20\ \mu\text{m}$ to $100\ \mu\text{m}$ diameter [2,4,7,8]. However, the range of TPB lengths from the gwd cathodes in these studies was limited due to inhomogeneous potential distributions that arise due to current collection problems. Various current collection techniques were used in these studies, but each was unable to offer the compromise of allowing molecular oxygen to access the LSCF and ensure a homogeneous potential distribution, which implies a uniform coverage by the current collector. In fact Prestat et al. achieved this compromise using a porous LSCF current collector [4], but then it is difficult to assess the contribution of the current collector to the oxygen reduction kinetics.

* Corresponding author.

E-mail address: n.simrick06@imperial.ac.uk (N.J. Simrick).

Literature on photolithography and etching processes are still lacking, especially for metal oxide structuring such as LSCF. These are two important steps in the fabrication process irrespective of the cathode material used since the reproducibility is vital for mechanistic studies and for potential micro-SOFC cathodes. Baumann et al. [8] describe the fabrication process of gwd LSCF films in some detail, but details of the etch rates are not given.

This paper addresses the fabrication of micro LSCF cathodes since standard photolithography and etching techniques borrowed from

the silicon-based microelectronics industry are not necessarily applicable to each stage of the fabrication process using SOFC materials. The main objective of this study is to develop a process for producing patterned thin film LSCF cathodes for fundamental studies of SOFC cathode mechanisms and possible use in micro SOFCs. Different etching routes are discussed – namely, dry versus wet etching. Furthermore, the impact of micro-fabrication via photolithography and etching in contrast to shadow mask processing on the electric properties of LSCF films is presented.

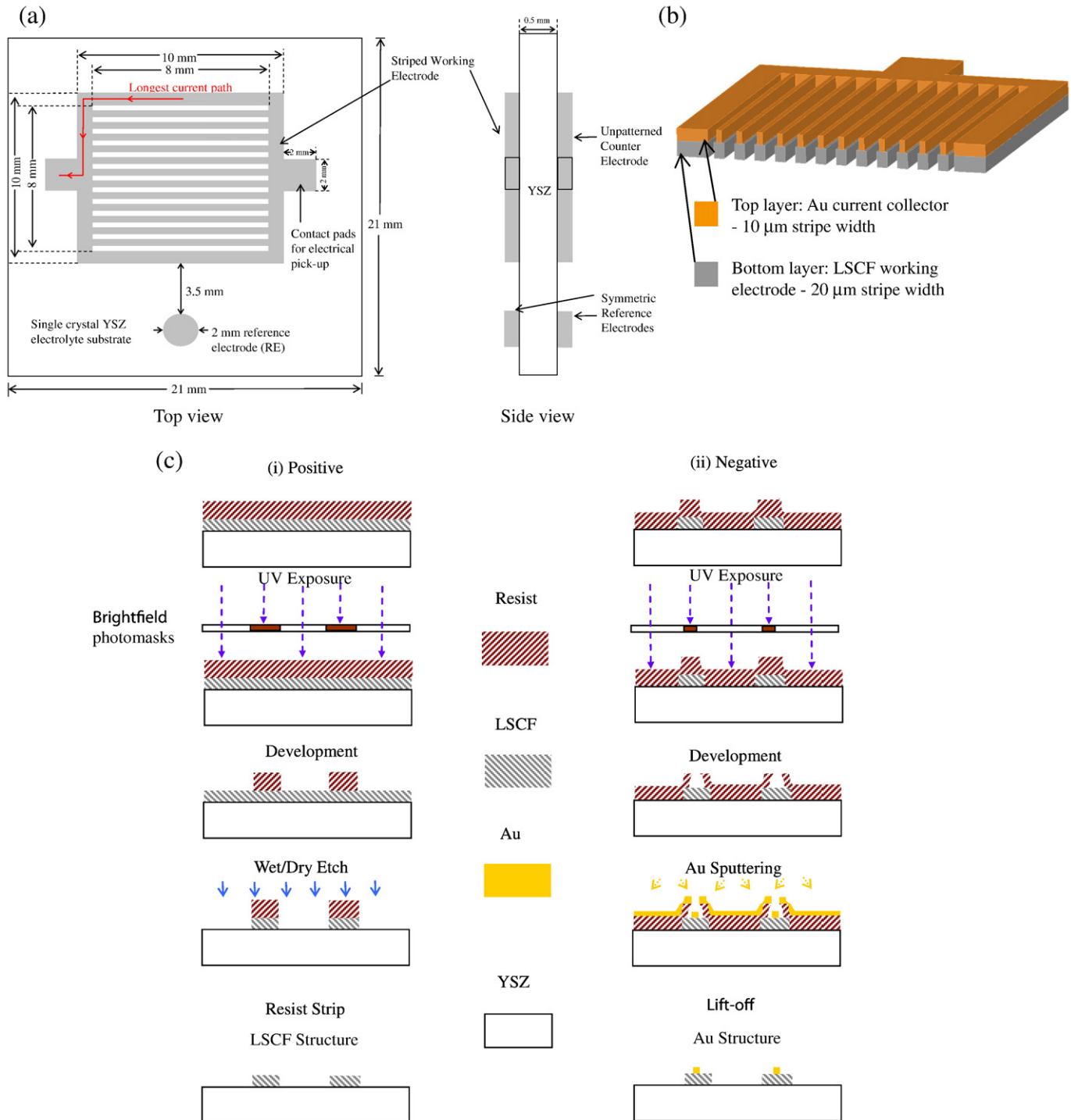


Fig. 1. Schematic representation of the cathode design shown without the current collection layer in (a) and with current collection in (b). Note in (b) the relative thicknesses are ~300 nm LSCF and ~365 nm Au. A flowchart of the micro-fabrication process is shown in (c). The sequence of steps for LSCF and Au patterning are shown in (c) (i) and (ii) respectively, with (ii) occurring after (i).

Table 1
Summary of geometrically well-defined photomask patterns and LSCF thickness.

Sample	LSCF stripe/ gap width [μm]	Effective LSCF area coverage ^a [cm^2] 2-d/3-d	LSCF I_{TPB} [m/cm^2]	LSCF thickness [nm]	Au stripe/ gap width [μm]	Au I_{TPB} [m/cm^2]
Cathode 1	330/330	0.158/0.159	0.264	290	165/495	0.268
Cathode 2	110/110	0.158/0.160	0.648	290	55/165	0.652
Cathode 3	20/20	0.159/0.169	3.26	290	10/30	3.26
Cathode 4	130/20.5	0.276/0.278	0.914	290	65/85.5	0.921
Cathode 5	50/100	0.106/0.109	0.923	290	25/125	0.925
Cathode 6	20/130	0.042/0.045	0.926	290	10/140	0.927
Cathode 7	110/110	0/0.003	0.648	470	110/110	0.648
Cathode 8	110/110	0/0.002	0.648	290	110/110	0.648
Cathode 9	110/110	0/0.0008	0.648	125	110/110	0.648
Cathode 10	8000/0	0.482	0.048	290	165/495	0.268
Cathode 11	8000/0	0.481	0.048	290	10/30	3.26
Cathode 12	20/20	0.758/0.768	3.26	290	0/0	0

^a Effective LSCF area is the LSCF uncovered by Au.

2. Experimental

LSCF thin films were prepared on (double-sided) epi-polished 9.5 mol% Y-doped 0.5 mm thick, 21 mm \times 21 mm yttria stabilized zirconia (YSZ) (100) single crystals in a three-electrode geometry for electrochemical evaluation. Single-crystal YSZ was used as a well-defined electrolyte substrate. Prior to deposition, the YSZ substrates were cleaned in a mixture of hydrogen peroxide and sulphuric acid ($\text{H}_2\text{O}_2:\text{H}_2\text{SO}_4$, 1:3 respectively), rinsed in deionised water and dried using filtered compressed nitrogen. All LSCF films (i.e. working, counter and reference electrodes), were laser-ablated from a $\text{La}_{0.6}\text{Sr}_{0.4}\text{Co}_{0.2}\text{Fe}_{0.8}\text{O}_{3-\delta}$ target which was uniaxially and then isostatically pressed from powder (Praxair) and sintered at 1250 °C for 4 h with 3 °C/min and 5 °C/min heating and cooling applied respectively. A pellet with greater than 95% of the theoretical density was formed. Thin films between 100 nm and 470 nm thick were deposited at a substrate temperature of 600 °C in 100 mTorr of oxygen with a pulse frequency of 10 Hz and fluence of 2.95 J/cm² (95 mJ) laser energy into 1.4 \times 2.3 mm spot size) using a KrF 248 nm excimer laser (SURFACE) and the films were cooled to room temperature under vacuum conditions (3×10^{-3} mTorr) at 10 °C/min. The target-to-substrate distance was 8.5 cm to ensure a relatively homogeneous film ($\pm 5\%$ at 400 nm) over 0.8 cm², which resulted in a deposition rate of approximately 1.28 nm/pulse.

As-deposited films were characterised by scanning electron microscopy (SEM, LEO 1530) and x-ray diffraction (XRD, SIEMENS Kristalloflex Diffraktometer D5000, step size/time per step of 0.02°/16 s) with focused ion beam (FIB, Zeiss NVision 40) utilised to produce cross-sections.

LSCF films were patterned within 1 cm² areas to produce gwd model cathode structures consisting of a series of stripes and gaps using photolithography and etching in a class 1000 cleanroom. A schematic of the design is shown in Fig. 1(a) and (b). The design parameters of the photomask (Delta Mask) used are summarised in Table 1 along with the LSCF film thickness, which was determined by SEM, FIB and surface step profiling (Alpha-Step 500) techniques. A Karl Suss MA6 Mask Aligner was used for the alignment of the photomask patterns to the substrate. The micro-fabrication process is shown in Fig. 1(c). Positive photoresist (microchemicals AZ 1518) and

negative photoresist (micro resist technology GmbH, ma-N 1410) were used for positive and negative processes respectively. It was necessary to remove the photoresist that built up at the edges and corners of the sample prior to the main exposure, either by an additional exposure/development step or using a swab. Positive and negative photoresists were developed in AZ 726 MIF (microchemicals) and ma-D533s (micro resist technology) respectively in a new batch of the developer solution for consistency. Films were rinsed for 30 s in deionised water and dried with filtered nitrogen. A final flood exposure of the positive photoresist for 1 min was performed after the photolithography process to deactivate it from further exposure. A systematic study of the photolithography parameters was performed to produce resist structures that were an accurate reproduction of the mask design. The optimal photolithography 'recipe' i.e. parameters used to define the positive photoresist mask are summarised in Table 2. LSCF was dry etched using argon ion (Ar^+) sputtering (RIE 76) with an initial base pressure of 9×10^{-5} mb, an Ar atmosphere of 1.00×10^{-1} mb, 200 W radio frequency power, 400 V DC bias, whilst maintaining the substrate at 10 °C. Sample placement within the chamber can vary the etch rate by up to 10%. Therefore samples were placed in the same position between etching cycles. Etching times up to 300 min were used for the 470 nm thick LSCF films in 20 min etch steps with 1 min Ar flow (50 sccm, 5.00×10^{-2} mb) between each step to prevent overheating/burning of the photoresist. LSCF was wet-etched in a diluted HCl solution ($\text{HCl}:\text{H}_2\text{O}$ 1:2) and thoroughly rinsed. The optimised etching parameters are shown in Table 3, including the dry etching of YSZ (100) single crystal, which proved to be a good etch stop with an etch rate approximately 3 times lower than that of the LSCF. A negative photoresist lift-off process was used to realise minimum stripe widths of 10 μm in the current collector. The analogous photolithography recipe is shown in Table 2.

Gold current collector stripes were fabricated centrally along each previously fabricated LSCF working electrode (WE) stripe with half the LSCF stripe width and also over the LSCF outer-frame and electrical pickup contacts. Gold was sputtered in an Ar atmosphere of 5×10^{-2} mb with 60 mA current and deposition rate 0.46 nm/s yielding 365 nm thick films. A minimum undercut of 1 μm in the negative photoresist was produced for successful lift-off in acetone at 50 °C for 30 min with minimal ultrasonic agitation. In order to exactly cover or 'cap' each LSCF stripe, the LSCF and Au films were protected with a single photoresist mask and dry etched simultaneously. LSCF was post-etched in an O_2 plasma and post-annealed at 500 °C to remove/burn-off residual photoresist.

The working and counter electrodes (CE) were made symmetric to each other ($\pm 20 \mu\text{m}$ i.e. within 10% of electrolyte thickness) in a three-electrode configuration using a circular reference electrode of 2 mm diameter, separated from the working electrode by 3.5 cm ($>3 \times$ electrolyte thickness). This was to reduce electrochemical measurement errors later by ensuring the reference electrode is at a known potential and minimising the misalignment between WE and CE [7,9,10].

3. Results and discussion

3.1. Film microstructure

Prior to the patterning process, LSCF thin films were characterised using XRD and SEM. As-deposited films (Fig. 2) were continuous and

Table 2
Summary of optimised photolithography recipes for positive and negative photoresists.

Photoresist	Dehydration Temp [°C]/time [min]	Pre-spin speed [rpm]/time [s]	Main-spin speed [rpm]/time [s]	Soft bake temp [°C]/Time [s]	Main exposure [mJ]/cm ²	Development time [s]	Hard bake temp [°C]/time [s]
AZ1518 (+ ve)	180/10	3000/3	4000/30	100/120	73.6	60	100/50
ma-N1410 (- ve)	180/10	2000/3	3000/30	120/90	390	90	-

Table 3
Summary of wet and dry etching parameters obtained in the study.

Material	Etch type	Etch rate
Single-crystal YSZ	Dry – Ar ⁺ sputtering	1.1 nm/min
Si ₃ N ₄	Dry – Ar ⁺ sputtering	4.04 nm/min
La _{0.6} Sr _{0.4} Co _{0.2} Fe _{0.8} O _{3–δ}	Dry – Ar ⁺ sputtering	3.4 nm/min–3.1 nm/min
La _{0.6} Sr _{0.4} Co _{0.2} Fe _{0.8} O _{3–δ}	Wet – HCl:H ₂ O (1:2)	400 nm/min

crack-free with negligible evidence of particle deposition during the laser ablation process. A difference in microstructure was observed depending on thickness. Films below a thickness of approximately 100 nm showed grains elongated in the film plane (i.e. grains with a larger aspect ratio upon viewing the surface) and in cross-section appeared dense (Fig. 2(a) and (c)). Burke et al. [11] showed that thin films with a grain size in the same range as its thickness may result in restricted grain growth. It is interesting to note that films with roughly 3 times larger film thicknesses of around 300 nm showed the characteristic columnar growth expected from the PLD process when viewed in cross-section, with grains appearing triangular upon viewing the surface, corresponding to the peaks of the columns and giving rise to an increased surface roughness (Fig. 2(b) and (d)). Films above 100 nm thick were observed to be slightly porous with approximately 30 nm separation between columns when FIB sections were produced (Fig. 3(a)).

XRD showed as-deposited films to be crystalline with peak positions corresponding to those reported previously for LSCF films [12,13], but the (012) peak was not observed (Fig. 4). A dependence on film thickness for the relative intensity of peak positions was observed indicating the reduction of texture with film thickness from

the initial preferred orientation on the (110) plane. No change in the XRD pattern was observed on post-annealing at 600 °C/4 h.

3.2. Film etching and patterning

LSCF patterned films were fabricated using two different etching processes, one wet and one dry. Wet etching using diluted HCl provided a fast etch rate of approximately 400 nm/min. Since the film thickness is only 100 to 300 nm this process is hard to control for fine etching towards the substrate. LSCF films were shown to readily over-etch with the observation of an undercut greater than the film thickness in the extreme case (Fig. 3(b)). This is undesirable for patterning, as it resulted in LSCF stripe widths less than the optimised photoresist stripe width. Considerably roughened edges also resulted, but the protected LSCF remained adhered to the YSZ substrate. There was no detectable etching of the YSZ single crystal, which remained stable during the etching process.

Dry etching resulted in an improved edge profile with a maximum contact angle of 75° to the substrate (Fig. 3(a)). The edge profile was less rough than for the HCl etch, but due to extended etching periods up to 300 min (LSCF etch rate of 3.4 nm/min, Table 3), photoresist and/or re-deposited LSCF was shown to remain at the microstructured stripe edge after multiple removal attempts (Fig. 3(c)). Heat treatment in air at 500 °C for 4 h removed most of the remaining material as seen in the FIB secondary electron image in Fig. 3(a). Heat treatment up to 600 °C (the deposition temperature) had little effect on the microstructure or XRD patterns of the LSCF thin films. The FIB section of the structured LSCF shows a thin dense layer with additional columnar growth. The dry-etched LSCF yielded structures closest to the original photomask design. Therefore, dry etching was

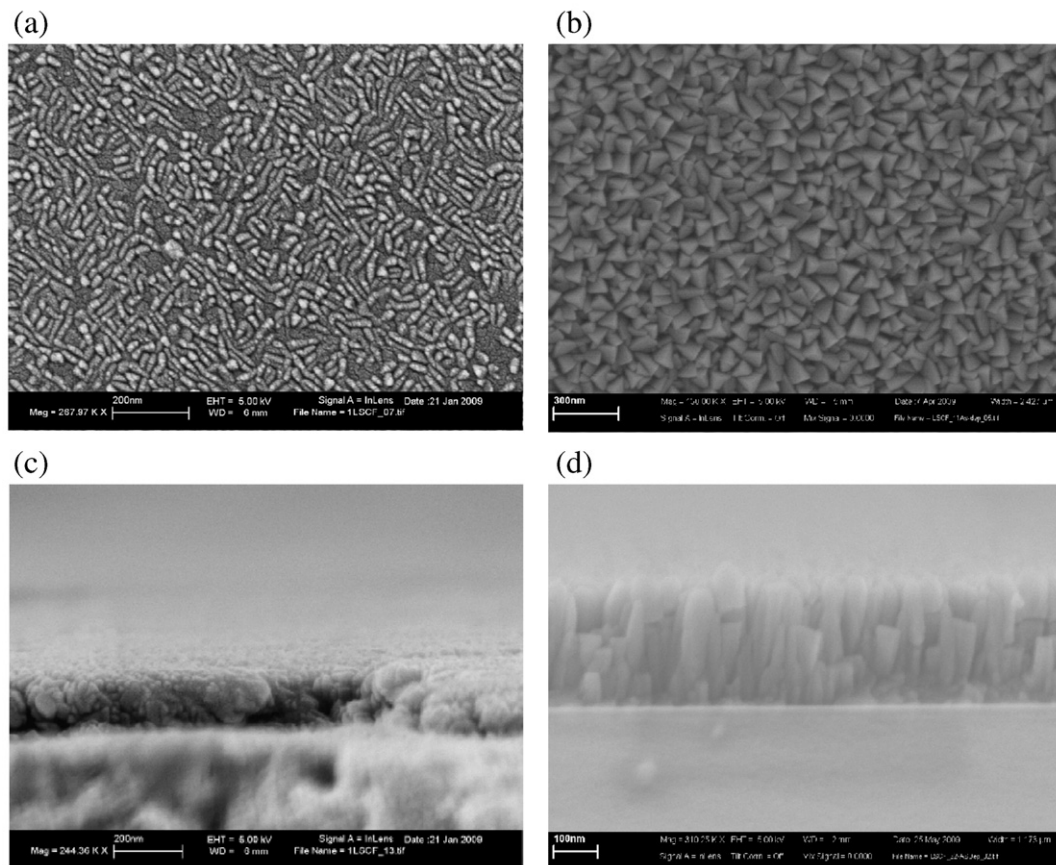


Fig. 2. Surface view SEM images of as-deposited films 100 nm and 300 nm thick in (a) and (b) respectively with their fracture cross-sections shown in (c) and (d) respectively. Triangular-like grains are observed for thicker films corresponding to the top of individual columns.

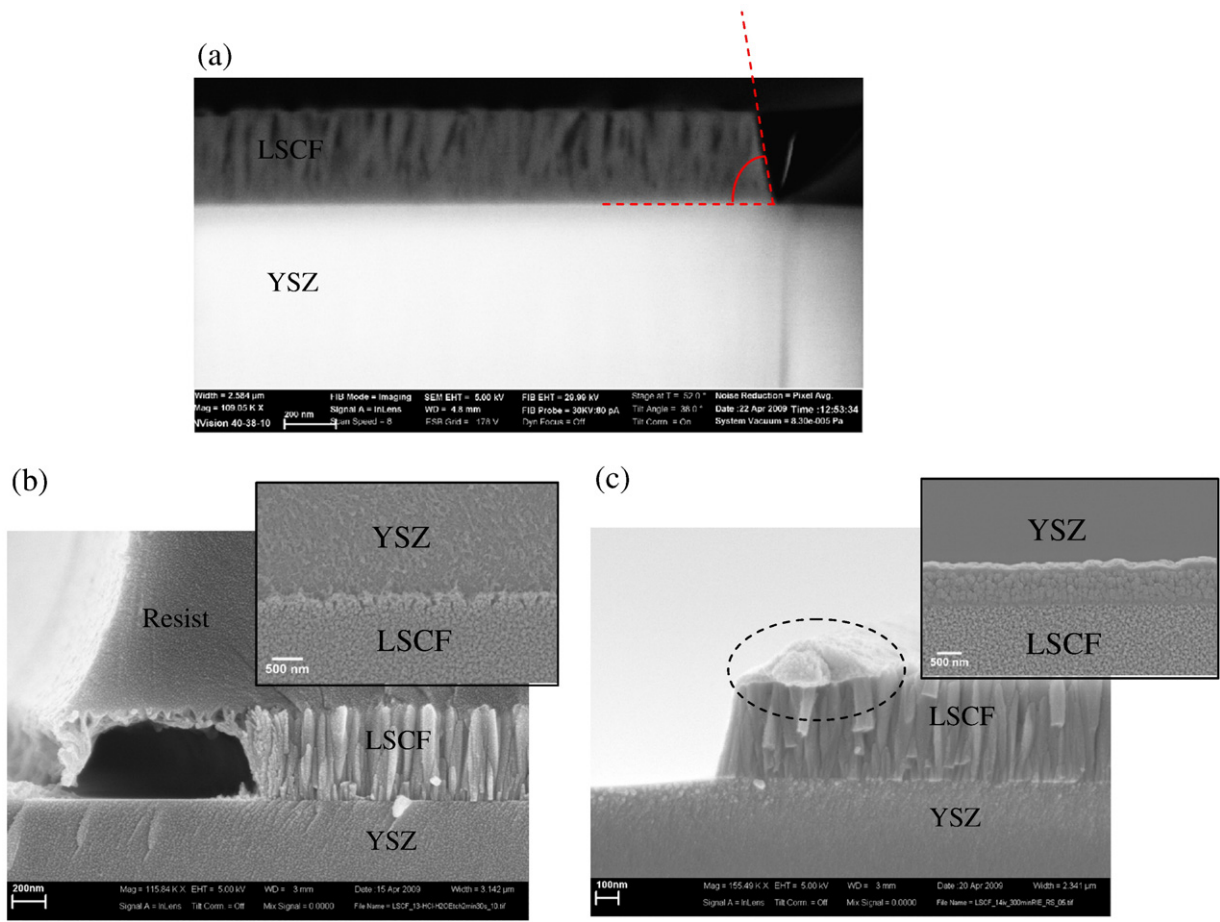


Fig. 3. FIB section of a LSCF stripe edge profile after dry etching and heat treatment (a). As-etched cross-sections of the LSCF stripe edge are shown in the case of (b) wet etching and (c) dry etching with the top view shown inset.

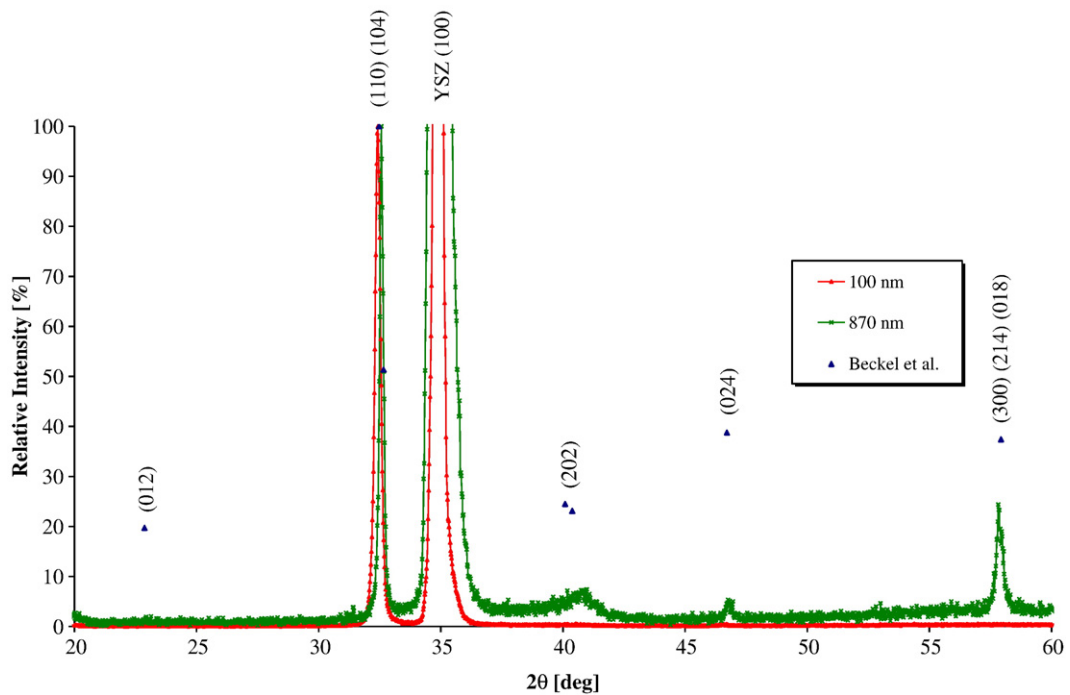


Fig. 4. XRD spectra of as-deposited LSCF thin films with peak positions from [13] and a thin-film reference [12] spectra superimposed.

the method chosen to produce gwd cathodes in this study. Etch rates are summarised in Table 3. The etch rate of single crystal YSZ was approximately 3 times less than the LSCF at 1.1 nm/min (Table 3). As a result a few nm of YSZ was etched between LSCF stripes. A similar result is reported by Baumann et al [8].

3.3. Conductivity measurements

Due to the relatively low electronic conductivity of bulk LSCF (30700 S/m at 600 °C) [14] and reduced cross-sectional area ($\sim 5.8 \times 10^{-12} \text{ m}^2$) of LSCF structures in this study, a novel gold Au current collection geometry was employed to achieve a homogeneous potential over the LSCF cathode during electrochemical measurements. It has been reported by Das et al. [15] that the effect of the electrode sheet resistance is significant and may result in considerable errors in the polarisation resistance measured. The requirement is that the potential drop over the electrode should be much less than the potential over the LSCF cathode/YSZ interface, which is the measurement in question. Assuming a typical AC amplitude of 10 mV, this is the upper limit of the potential drop permitted. Finite element analysis using COMSOL Multiphysics 3.4 confirmed the necessity of the Au current collector structured along each LSCF stripe to reduce the potential drop from the furthest stripes to the two electrical pickup points on the outer-frame. A basic 3-dimensional DC model consisting of the LSCF with and without the Au current collection of assumed conductivity $45.2 \times 10^6 \text{ S/m}$ was compared. It was found that the potential drop between the furthest LSCF stripe and the electrical pickup would be reduced from 300 mV to 0.2 mV when the current collector is applied.

An example of a patterned LSCF cathode and Au current collector is shown in Fig. 5(a). A closer view of the finest (20 μm wide) LSCF stripe complete with (10 μm wide) Au current collector on top is shown in Fig. 5(b). A misalignment between the LSCF and Au of less than 5 μm was achieved. The LSCF stripes were ‘capped’ by Au by etching through the Au and LSCF un-patterned films in a single dry etching cycle i.e. using a single photolithography step. The Au uniformly covers the LSCF up to the stripe edge leaving the LSCF ‘wall’ thickness visible as required (Fig. 5(c)). This is important since the aim is to use this design to correlate the electrochemical performance i.e. polarisation resistance with the area of LSCF defined only by the thickness. As the number of stripes increases, so too does the total surface area of the film edges. In the case of 20 μm wide LSCF stripes, the additional surface area from the stripe side walls is approximately 6% (Table 1).

The electrical conductivity in static air of an as-deposited LSCF film deposited through a 1 cm^2 shadow mask was compared with LSCF patterned into the same 1 cm^2 geometry using photolithography and dry etching in geometry-corrected four-point Van der Pauw measurements. Neither film was heat treated prior to testing, but during the photolithography process substrates were placed onto a hotplate with a maximum temperature of 180 °C for dehydration prior to the application of photoresist. A color change (darkening) in the LSCF was always evident after dehydration, possibly related to an increase the oxygen content [16]. This characteristic color change was observed after the photolithography and etching process. However, electrical measurements were initiated after equilibration at 600 °C and cooling to room temperature and the results are shown in Fig. 6. The conductivity and activation energy of the LSCF film deposited through the shadow mask were observed to be different from those of the lithographically processed film, mainly at temperatures below 400 °C

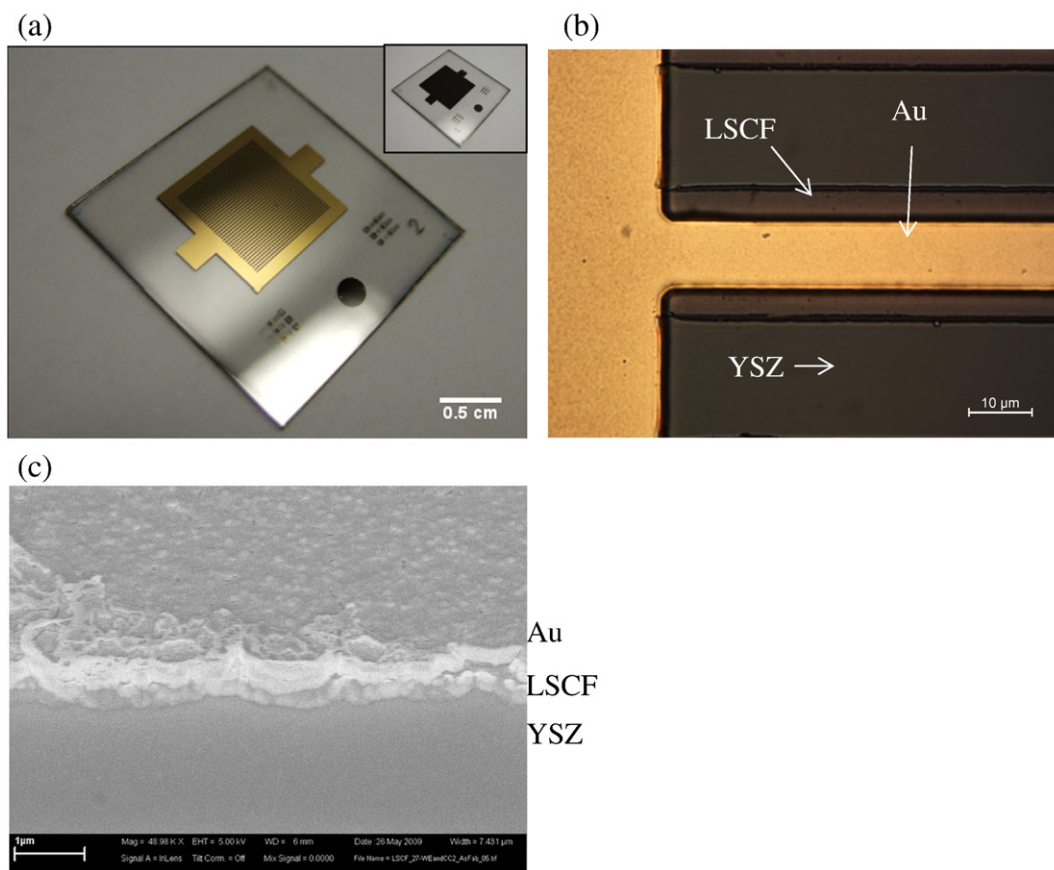


Fig. 5. The working electrode side of a completed cell is shown in (a) with the counter electrode (unstructured without Au current collection) shown inset. An as-fabricated 20 μm LSCF stripe with integrated Au current collector (10 μm) is shown in (b). The result of simultaneously etching the Au and LSCF stripes is shown in (c) with the Au completely covering the (top) LSCF surface whilst leaving the LSCF side wall exposed.

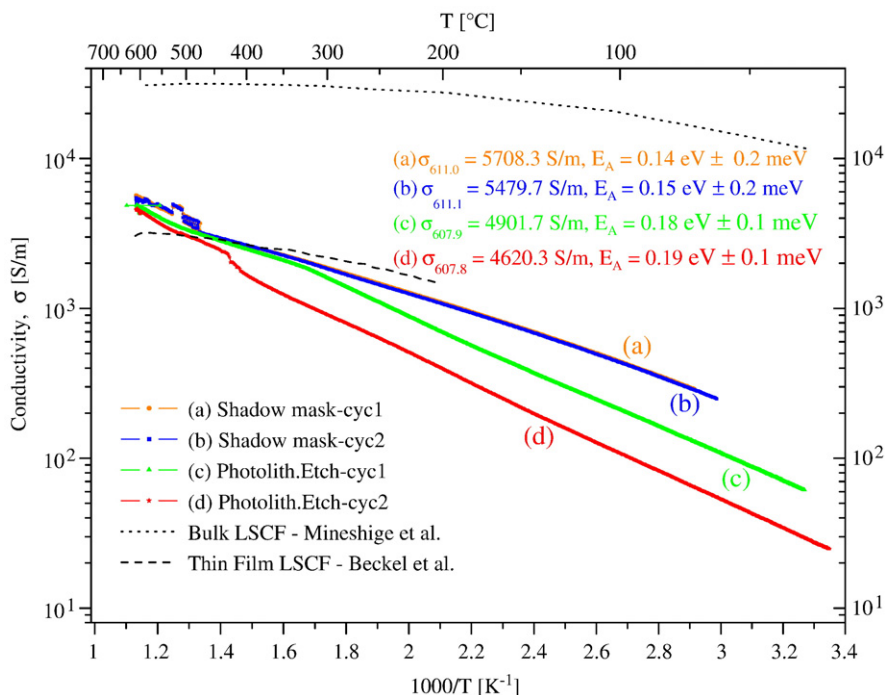


Fig. 6. Electrical conductivity of LSCF thin films 220 nm thick, deposited through a shadow mask and 290 nm thick, produced via photolithography and etching in (a, b) and (c, d) respectively during cooling at 3 °C/min over two temperature cycles. Both films were deposited on single-crystal YSZ substrates. Activation energies were calculated from the data obtained at 350 °C and lower, where a better fit was obtained. Comparison to bulk LSCF [14] and thin film LSCF [17] is also shown.

(Fig. 6). The shadow mask processed LSCF films show no degradation on cycling whereas the lithographically processed films do. These differences may be related to an effect occurring during photolithography or the color change observed in the material during this process.

An investigation of the LSCF microstructure after the experiments revealed no significant difference in grain sizes, except the grains of the unprocessed film seemed to be arranged more orderly i.e. mostly either parallel or perpendicular to each other, with a higher aspect ratio.

The highest conductivity observed at 600 °C is 5 times lower than previously reported for bulk LSCF [14], but consistent with LSCF thin films deposited by spray pyrolysis on sapphire substrates [17]. The maximum measured conductivity value of 5700 S/m is slightly greater than the 3200 S/m obtained by Beckel et al. [12] for films deposited by spray pyrolysis with 2% porosity and annealed at the same temperature. However the corresponding activation energy of 0.14 eV in this study is nearly 3 times greater. In fact, the activation energies in this study correlate better with the sprayed films annealed at higher temperatures, with 19% porosity in the study by Beckel et al [12].

4. Conclusions

$\text{La}_{0.6}\text{Sr}_{0.4}\text{Co}_{0.2}\text{Fe}_{0.8}\text{O}_{3-\delta}$ thin films between 100 and 300 nm thick were deposited on different single-crystal yttria-stabilised zirconia (YSZ) electrolyte substrates. As-deposited LSCF films thinner than 100 nm were dense and thicker films showed additional columnar growth with some possible porosity between columns. The thin films were patterned using photolithography and both dry and wet-etched. Wet etching resulted in undercutting of the thin-film and rough edge profiles. Conversely, dry etching resulted in side walls inclined at 75° to the substrate and was the chosen method to produce the geometrically well-defined model cathode structures for future electrochemical studies. Gold current collectors were deposited either centrally along each LSCF stripe or over the entire LSCF surface in

order to produce structures that could be used to determine a correlation of performance with electrode geometry. The electrical conductivity of the LSCF showed a maximum of 5700 S/m at 600 °C, considerably less than the bulk material. It was found that LSCF thin-film structures processed via photoresists and etching exhibit degradation of electric conductivity upon thermal cycling. However, LSCF films deposited through shadow masks showed no similar degradation. Future work will entail the electrochemical characterisation of the electrodes produced by these processes in order to better understand the oxygen reduction mechanism at LSCF cathodes at the relatively low temperatures that are used in micro SOFCs.

Acknowledgements

The author wishes to thank the EPSRC for the DTA studentship funding, Prof. Gauckler of Dept. of Nonmetallic Inorganic Materials ETH Zürich for the use of equipment facilities and the IDEA League for the travel grant to complete this work.

References

- [1] S.J. Skinner, *International Journal of Inorganic Materials* 3 (2) (2001) 113.
- [2] F.S. Baumann, J. Fleig, H.-U. Habermeier, J. Maier, *Solid State Ionics* 177 (11–12) (2006) 1071.
- [3] S. Wang, M. Katsuki, M. Dokiya, T. Hashimoto, *Solid State Ionics* 159 (1–2) (2003) 71.
- [4] M. Prestat, A. Infortuna, S. Korrodi, S. Rey-Mermet, P. Murali, L. Gauckler, *Journal of Electroceramics* 18 (1) (2007) 111.
- [5] D. Beckel, A. Bieberle-Hütter, A. Harvey, A. Infortuna, U.P. Muecke, M. Prestat, J.L. M. Rupp, L.J. Gauckler, *Journal of Power Sources* 173 (1) (2007) 325.
- [6] A. Evans, A. Bieberle-Hütter, J.L.M. Rupp, L.J. Gauckler, *Journal of Power Sources* 194 (1) (2009) 119.
- [7] D. Beckel, U.P. Muecke, T. Gyger, G. Florey, A. Infortuna, L.J. Gauckler, *Solid State Ionics* 178 (5–6) (2007) 407.
- [8] F.S. Baumann, J. Fleig, G. Cristiani, B. Stuhlhofer, H.U. Habermeier, J. Maier, *Journal of The Electrochemical Society* 154 (9) (2007) B931.
- [9] J. Rutman, I. Riess, *Solid State Ionics* 179 (21–26) (2008) 913.
- [10] S.B. Adler, *Journal of The Electrochemical Society* 149 (5) (2002) E166.
- [11] J.E. Burke, D. Turnbull, *Progress in Metal Physics* 3 (1952) 220.

- [12] D. Beckel, A. Dubach, A.N. Grundy, A. Infortuna, L.J. Gauckler, *Journal of the European Ceramic Society* 28 (1) (2008) 49.
- [13] J.E. ten Elshof, J. Boeijsma, *Powder Diffraction* 11 (3) (1996) 240.
- [14] A. Mineshige, J. Izutsu, M. Nakamura, K. Nigaki, J. Abe, M. Kobune, S. Fujii, T. Yazawa, *Solid State Ionics* 176 (11–12) (2005) 1145.
- [15] R. Das, D. Mebane, E. Koep, M.L. Liu, *Solid State Ionics* 178 (3–4) (2007) 249.
- [16] M. Søgaard, *Transport Properties and Oxygen Stoichiometry of Mixed Ionic Electronic Conducting Perovskite-type Oxides*, Risø National Laboratory, Roskilde, Denmark, 2006.
- [17] D. Beckel, D. Briand, A. Bieberle-Hutter, J. Courbat, N.F. de Rooij, L.J. Gauckler, *Journal of Power Sources* 166 (1) (2007) 143.